**Magnesium Technology 2011**
*Edited by: Wim H. Sillekens, Sean R. Agnew, Neale R. Neelameggham, and Suveen N. Mathaudhu*
***TMS (The Minerals, Metals & Materials Society), 2011***

# STRUCTURE AND MECHANICAL PROPERTIES OF MAGNESIUM-TITANIUM SOLID SOLUTION THIN FILM ALLOYS PREPARED BY MAGNETRON-SPUTTER DEPOSITION

Daad Haddad[1], GuangLing Song[2*], Yang Tse Cheng[3]
[1]MEDA Engineering and Technical Services LLC; 17515 W. Nine Mile Road; Southfield, MI 48075, USA
[2]Chemical Sciences and Materials Systems Lab, GM Global Research and Development; 30500 Mound Road; Warren, MI 48090, USA
[3]Department of Chemical and Materials Engineering, University of Kentucky; 177 F. Paul Anderson Tower; Lexington, KY 40506, USA

Keywords: Magnetron Sputtering, Mg-Ti thin films, Nanoindentation, X-ray diffraction, Atomic Force Microscopy

## Abstract

Mg alloys are being considered for wider application in automotive industry. Designing new alloys with improved mechanical properties is important to the development of new Mg alloy parts. Mg-Ti is an interesting alloying system that may have good corrosion resistance due to high passivity of Ti. However it is difficult to form through a conventional metallurgical method due to the mutual insolubility of Mg and Ti and the big difference in their melting point. Nevertheless, if the alloy can be formed, it may have other unexpected physical and chemical performance. Therefore, it is of significance to understand the properties of Mg-Ti alloy produced by non-conventional approach.

In this report, $Mg_{(1-x)}Ti_x$ thin film alloys containing 0, 21, 41, 51, 58, 81 and 100 at.% Ti were deposited by dc magnetron sputtering on Si substrates. The mechanical properties of the thin film alloys were obtained using nanoindentation. Electron probe microanalysis (EPMA) was used to determine the film compositions. X-ray diffraction (XRD) measurements showed that single phase magnesium-titanium solid solutions were obtained across the full range of magnesium and titanium mixtures. The topography and the rms roughness of the different alloys were studied using atomic force microscopy (AFM). The mechanical properties of the $Mg_{(1-x)}Ti_x$ thin films were determined by analyzing the nanoindentation load-displacement curves based on the Oliver-Pharr method. The nanoindentation results show that both the elastic modulus and hardness of the $Mg_{(1-x)}Ti_x$ alloy thin films are higher than those of conventional Mg alloys.

## Introduction

Magnesium and magnesium alloys have attracted wide attention as lightweight materials that can be used in automotive, aerospace, and hydrogen storage applications. The alloying of magnesium and titanium is of particular interest due to the improved mechanical and corrosion resistant properties of Ti [1-5]. However, magnesium and titanium have very little mutual solubility according to their equilibrium phase diagram, and thus do not form any stable intermetallic compounds under standard alloying conditions [6, 7]. But recently it was reported that by using non-standard alloying techniques, such as electron-beam deposition and magnetron sputtering, the solid solubility of Mg and Ti can be extended significantly and solid solution $Mg_{(1-x)}Ti_x$ thin film alloys can be formed [8-15]. These $Mg_{(1-x)}Ti_x$ films are expected to have the advantages of being lightweight alloys with high specific strength and better corrosion performance.

In this work, the fabrication of $Mg_{(1-x)}Ti_x$ thin film alloys with different Ti content is presented. The topography and the crystal structure of these films are studied using AFM and XRD measurements. Finally, the mechanical properties of these films are measured using nanoindentation experiments and by analyzing the load-displacement curves based on the Oliver-Pharr method [16]. The effect of the composition and morphology on the mechanical properties of these alloys is discussed.

## Mg-Ti Thin Films Deposition

The $Mg_{(1-x)}Ti_x$ ($x \approx 0$, 0.21, 0.41, 0.51, 0.58, 0.81, 1) thin films were grown on 1″ Si (100) substrates using dc magnetron sputtering under argon atmosphere. The silicon substrates were ultrasonically cleaned in acetone and methanol successively for 20 minutes. The cleaned substrates were loaded in the load lock chamber where they were heated to 200°C for 30 minutes under vacuum for outgasing. After cooling down, the substrates were transferred to the growth chamber which has a base pressure of about $5.0\times10^{-8}$ Torr.

The deposition plasma for each constituent material was created utilizing a dc power source and a flow of Ar (14 sccm). The dynamic pressure during the growth of the films was 2 mTorr. Deposition of the different alloys is carried out using a recipe which depends on predetermined deposition rates. Growth rates of the magnesium and titanium sources were measured, under the above specified growth conditions, at different dc powers (50 – 600 W) using deposition monitor with the crystal sensor positioned just above the center of the substrate holder. For each composition, the ratio of Mg to Ti growth rate was calculated as a function of the ratio of Mg to Ti atoms. Using the measured growth rates and the calculated growth rate ratio, the film composition was controlled by changing the power to the Mg and Ti targets. The dc powers applied to each target during the deposition of the different alloys together with EPMA determined compositions are summarized in Table I. There is excellent agreement between the measured and calculated compositions. The substrates were rotated at 20 rpm in order to obtain uniform composition across the substrates. The films are typically 1.2-1.5 μm thick as determined from SEM cross section measurements.

## Materials Characterization

The composition of the different Mg-Ti thin film samples was determined using Electron probe microanalysis (EPMA). EPMA measurements were made with a Cameca Instruments, Inc. (Nampa, ID) model SX-100 electron probe. Analysis voltage and current were 15 keV and 10 nA. Analyses were done with a focused beam < 1.0 μm in diameter. Each sample was analyzed at 8 random locations with results averaged. Mg and Ti compositions were calculated from x-ray intensities (k-ratios) with the thin film

program GMRFILM [17]. Precision and accuracy are both estimated as +/- 2% relative for all samples.

Ex-situ X-ray diffraction was used to study the structures of the Mg-Ti films. Each sample was examined using Cu $K_\alpha$ radiation in a Bruker AXS General Area Detector Diffractometer System (GADDS). The diffraction images are typically collected for a period of 5 minutes using a 0.5 mm collimator and a sample to detector distance of 60 mm. The primary beam incidence angle is 17 degrees. Each diffraction scan was examined for incomplete Debye rings, which indicate preferred crystallite orientation, crystallite size in the film, and single crystal substrate diffraction peaks. Each diffraction image is then integrated to produce a powder diffraction pattern. The diffraction patterns are then compared to reference data for phase identification. Once phase identification is complete lattice parameters can be calculated.

Topography measurements of the Mg-Ti alloy samples were obtained using Dimension V Scanning Probe Microscope (Veeco). The height measurements were obtained using tapping mode and scanning area of 5.0 μm × 5.0 μm. The AFM measurements were performed in air, at ambient temperature and humidity, using a silicon probe with tip ROC (radius of curvature) < 10 nm. Four topography maps at different positions were acquired for each sample. The reported values of the rms roughness are the mean values of the different measurements.

Nanoindentation experiments were carried out with a Hysitron Triboscope (Hysitron Incorporated, Minneapolis, MN). The load controlled indents were made with a Berkovich indenter. The load function consists of three segments, a 5 seconds loading segment, a 2 seconds holding segment at the maximum load, and a 5 seconds unloading segment. Indents were made to a depth of about 10 percent of the film thickness to minimize substrate effects (typically ~140 nm). Data values are averaged from a series of 16 indents per sample. The hardness and modulus are calculated based on the Oliver-Pharr method [16].

Table I. The dc power applied to the Mg and Ti sources during deposition of $Mg_{(1-x)}Ti_x$ thin films at room temperature along with the corresponding Mg and Ti concentration calculated using measured growth rates and the concentration determined from EPMA measurements

| Sample | Power (W) | | Calculated Concentration (Using Growth rates) (at.%) | | Measured Concentration (EPMA) (at.%) | |
|---|---|---|---|---|---|---|
| | Mg | Ti | Mg | Ti | Mg | Ti |
| Mg | 100 | - | 100 | - | >99 | <1 |
| $Mg_{0.80}Ti_{0.20}$ | 100 | 130 | 80 | 20 | 79 | 21 |
| $Mg_{0.60}Ti_{0.40}$ | 50 | 200 | 60 | 40 | 59 | 41 |
| $Mg_{0.50}Ti_{0.50}$ | 50 | 300 | 50 | 50 | 49 | 51 |
| $Mg_{0.40}Ti_{0.60}$ | 40 | 310 | 40 | 60 | 42 | 58 |
| $Mg_{0.20}Ti_{0.80}$ | 20 | 450 | 20 | 80 | 19 | 81 |
| Ti | - | 300 | - | 100 | <1 | >99 |

## Results and Discussion

Crystallographic Structure

The microstructure of the $Mg_{(1-x)}Ti_x$ thin film alloys was determined by XRD measurements. The XRD patterns of the different Mg-Ti films after normalization are shown in Figure 1. The Mg film shows a very strong diffraction peak at 2θ ~ 34.8° which is due to the **(0002)** plane of hexagonal closed packed (HCP) Mg. The Mg film exhibits a strong preferential crystallographic orientation with the **(0001)** plane growing parallel to the substrate surface. The weak diffraction peaks at higher 2θ correspond to the HCP Mg **(10$\bar{1}$2)** and **(10$\bar{1}$3)** peaks. XRD pattern of the $Mg_{0.79}Ti_{0.21}$ thin film shows a strong diffraction peak at 2θ ~ 35.8° that is due to the **(0002)** plane of HCP solid solution unit cell. This peak is shifted to a higher angle (lower d-spacing) with respect to pure Mg due to the partial substitution of Mg atoms by Ti atoms. Because Ti has relatively smaller molar volume than Mg, partial substitution of Mg by Ti causes the Mg lattice to contract and thus d-spacing to decrease. The peak at higher 2θ is due to **(10$\bar{1}$3)** HCP Mg-Ti solid solution. Mg and $Mg_{0.79}Ti_{0.21}$ samples have a strong [001] fiber texture as reflected by the strong **(0002)** diffraction peak of the HCP Mg-Ti unit cell.

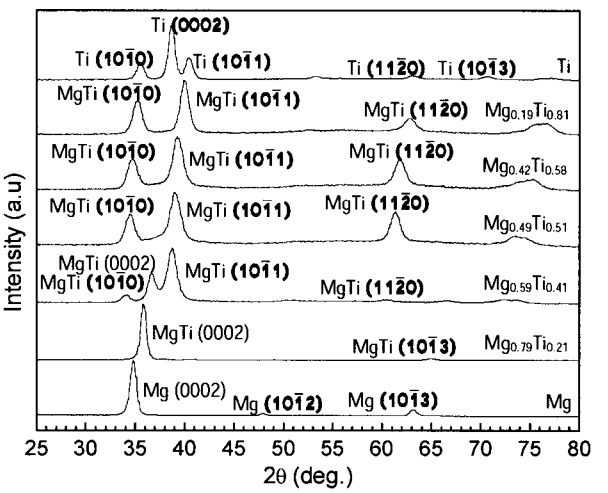


Figure 1. XRD spectra of $Mg_{(1-x)}Ti_x$ thin film alloys.

The film with 41 at.% Ti shows a single phase corresponding to HCP Mg-Ti solid solution. XRD pattern of this film shows three diffraction peaks at lower 2θ (~ 34.0°, 36.6°, and 38.7°) which are due to the **(10$\bar{1}$0)**, **(0002)**, and **(10$\bar{1}$1)** peaks of a contracted HCP Mg lattice with Mg atoms substituted by Ti. The $Mg_{(1-x)}Ti_x$ samples with x ~ 0.51, 0.58 and 0.81 show also a single phase with two diffraction peaks that can be attributed to the **(10$\bar{1}$0)**, and **(10$\bar{1}$1)** diffraction peaks in HCP Mg-Ti lattice. In all these films, the higher 2θ diffraction peaks correspond to the Mg-Ti HCP phase. The pure Ti film, unlike the Mg film, does not show one highly preferred orientation. The XRD spectra of Ti film show the **(10$\bar{1}$0)**,**(0002)**, and **(10$\bar{1}$1)** diffraction peaks of Ti HCP lattice at lower 2θ (35.5°, 38.6°, and 40.4 °).

The above XRD results suggest that all the Mg-Ti thin film alloys are a single hexagonal Mg matrix phase with various contents of Ti in the solid solution. The lattice of the Mg-Ti solid solution contracts with the addition of Ti. In Figure 2, the lattice constants of the $Mg_{(1-x)}Ti_x$ films calculated from XRD spectra are presented as a function of Ti content, x. Also shown in Figure 2 are the lattice constants at different composition calculated using Vegard's Law [18]. Accordingly, the lattice constants of the alloys are linearly interpolated from the values of the pure compounds using the following relation:

$$a_{A_{(1-x)}B_x} = (1-x)a_A + xa_B \quad (1)$$

The calculated lattice constants from XRD spectra agree with those predicted using Vegard's law confirming that a solid solution of Mg-Ti was obtained.

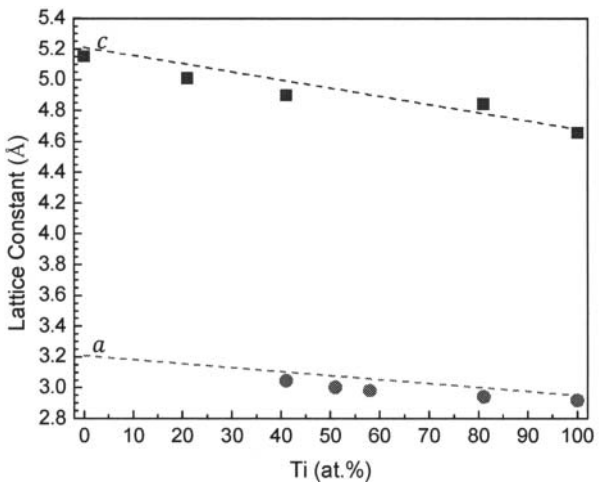


Figure 2. Dependence of lattice constants on the composition of the Mg-Ti samples. Also shown the linear dependence of lattice constants on the alloy composition predicted by Vegard's Law.

Topographic morphology

AFM height images of the Mg-Ti alloys are given in Figure 3. The pure Mg sample shows large hexagonal particles protruding from the film surface at different angles, and making the sample surface very rough. Figure 4 displays the root-mean-square (rms) roughness of the Mg-Ti thin films obtained from AFM height images as a function of Ti concentration. These results show that Mg thin film has a very high rms roughness of ~ 30nm. The AFM image of sample $Mg_{0.79}Ti_{0.21}$ shows that the large hexagonal particles disappeared and are replaced by small irregularly shaped particles that stretch along the sample surface. The refined almost-flat particles in sample $Mg_{0.79}Ti_{0.21}$ leave the surface of this sample significantly smoother with a much smaller rms roughness compared to Mg sample (Figure 4).

As the Ti concentration increases to 41, 51, and 58 at.%, **(10$\bar{1}$0)** and **(10$\bar{1}$1)** oriented Mg-Ti grains start to emerge in these films. AFM height images of these samples show also angular particles that stick out of the film surface. The appearance of these new **(10$\bar{1}$0)** and **(10$\bar{1}$1)** oriented Mg-Ti grains in these films affects the surface roughness of these films, which increases to a maximum value for the sample with 58 at.% Ti (Figure 4). The topography of the Ti-rich sample $Mg_{0.19}Ti_{0.81}$ shows long narrow rectangular stick-like particles. These particles grow evenly along the surface of the film and do not protrude out of the surface making the surface of this film smooth with small surface roughness compared to the films with 51 and 58 at.% Ti.

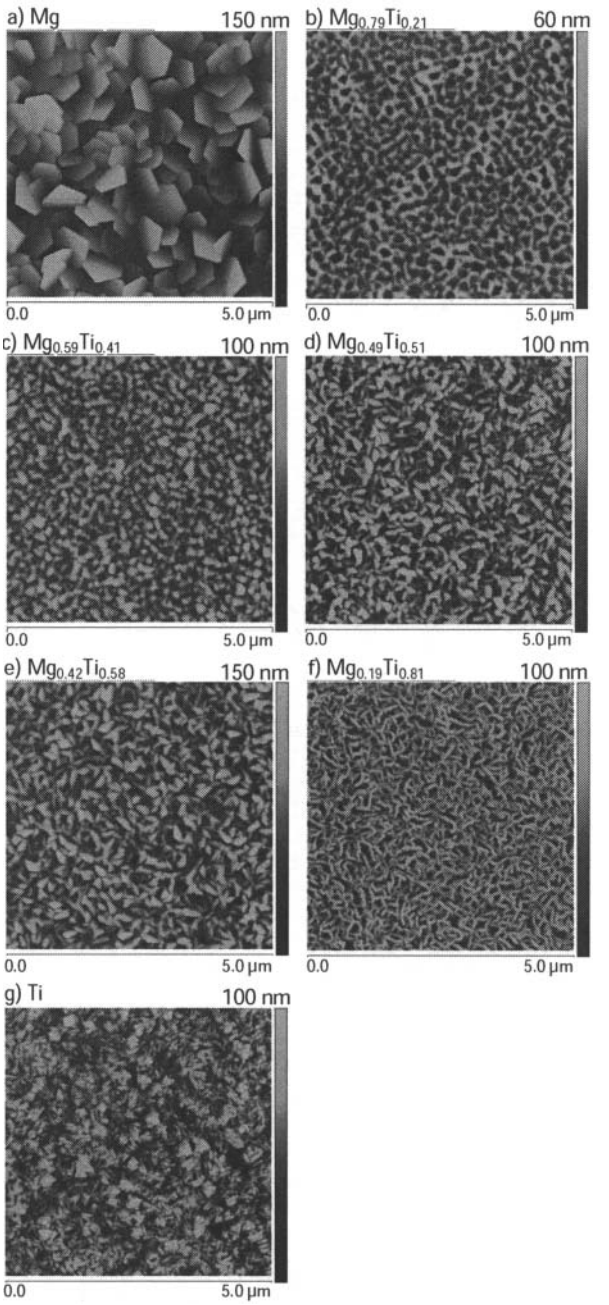


Figure 3. AFM topography images of the different Mg-Ti alloy thin films: a) Mg, b) $Mg_{0.79}Ti_{0.21}$, c) $Mg_{0.59}Ti_{0.41}$, d) $Mg_{0.49}Ti_{0.51}$, e) $Mg_{0.42}Ti_{0.58}$, f) $Mg_{0.19}Ti_{0.81}$, and g) Ti.

Finally, the pure Ti topography shows the fine rectangular stick-like shape as in $Mg_{0.19}Ti_{0.81}$ but in smaller size in addition to some coarse larger particles making the surface roughness of this film slightly higher than that of the $Mg_{0.19}Ti_{0.81}$ sample

The in-plane particle sizes of the different Mg-Ti samples were calculated using cross section analysis of the AFM height measurements and are presented in Figure 4. For each sample the measured lengths of 15 different particles along the short and long axes were averaged to give a mean value of the particle size of that sample. Mg sample shows large particle size of about ~ (750 ± 120) nm. The particle size value decreases to ~ 200 nm for the samples with Ti content of 21, 41 and 51 at.%, and then slightly increases to ~ (250 ± 80) nm for the $Mg_{0.42}Ti_{0.58}$ sample. For the Ti-rich sample (x = 0.81) the particle size decreases again to ~ (175 ± 90) nm reaching a minimum value of ~ (140 ± 40) nm for the pure Ti sample.

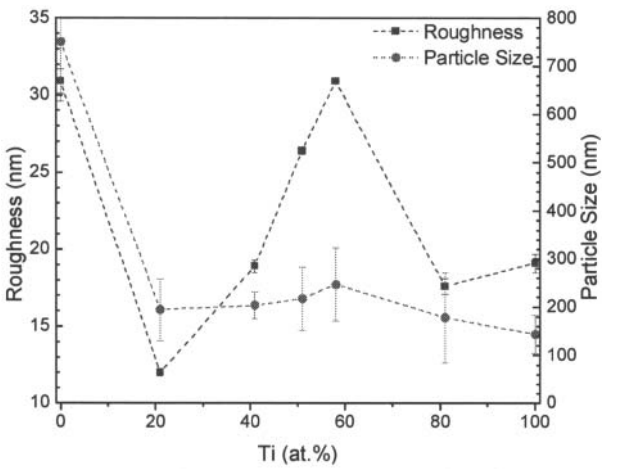


Figure 4. Root-mean-square (rms) roughness and particle size of Mg-Ti alloy thin films, obtained from AFM height images and displayed as a function of Ti concentration.

Micro-Mechanical Properties

The commonly used Oliver-Pharr method was used to analyze the indentation data and to calculate the Young's modulus and hardness of the Mg-Ti samples. According to this method, the hardness is defined as:

$$H = P_{max}/A_c \quad (2)$$

where $P_{max}$ is the maximum indentation load and $A_c$ is the projected contact area of the indenter tip at that load. The contact area of the indenter is calculated as a function of contact depth, $h_c$, using a series of indents at various loads (various $h_c$) performed on a sample with a known elastic modulus. Although this method does not account for the resulting indentation shape (e.g., pile-up) or the elastic mismatch between the film and the substrate it serves as a tool for estimating mechanical properties. The Young's modulus is obtained from:

$$E = 1/\gamma\left(\sqrt{\pi}/2\right)\left(S/\sqrt{A_c}\right) \quad (3)$$

where $\gamma$ is a correction factor that depends on the indenter geometry and S is the stiffness of the unloading curve given by the slope of the initial portion of the unloading curve.

A total of 16 indents are performed on each sample and the load was chosen so that the contact depth was ~ 140 nm to minimize substrate and roughness effects. The calculated mechanical properties of each sample are then averaged and the mean values of modulus and hardness are plotted in Figure 5 along with the standard deviations. The measured Young's modulus and hardness of pure Mg and Ti thin film samples clearly show, as expected, higher Young's modulus and hardness values of Ti sample over Mg sample. It is reasonable to expect the Young's modulus and hardness of the Mg-Ti alloys to increase monotonically with the addition of Ti. However, the results show that $Mg_{(1-x)}Ti_x$ samples with x = 0.21, and 0.81 have both similar Young's modulus and hardness. Actually, sample $Mg_{0.79}Ti_{0.21}$ shows very large improvement in mechanical properties compared to pure Mg sample. But, as Ti content increases to 41, 51, and 58 at.% the measured Young's modulus and hardness of the corresponding samples are lower than those of the Mg-Ti sample with 21 at.% Ti but higher than those of pure Mg sample.

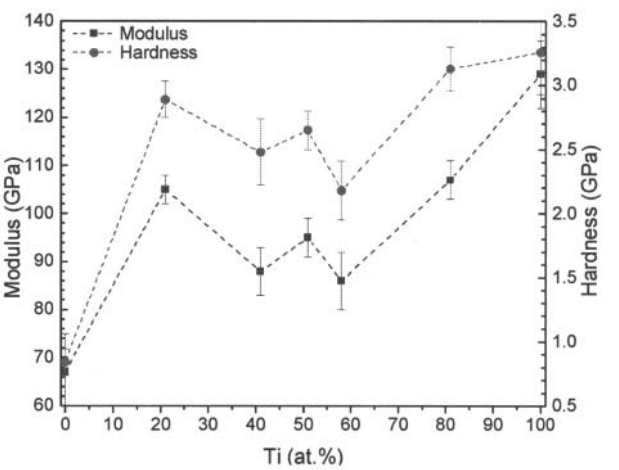


Figure 5. Calculated Young's modulus and hardness of the Mg-Ti alloy samples plotted as a function of Ti content.

These results can be understood once the effect of roughness on the measured modulus and hardness values is taken into account [19, 20]. This effect originates from the initial contact between the indenter tip and the rough surface when some flattening can occur causing the measured $h_c$ and thus $A_c$ to be less accurate. As a result the measured modulus and hardness of the Mg-Ti samples are affected by both the addition of Ti content which should result in improving mechanical properties and the increased surface roughness of the samples which would reduce the values of the modulus and hardness. The $Mg_{0.79}Ti_{0.21}$ shows a very small surface roughness compared to Mg sample, and as a result its mechanical properties are strongly improved due to both Ti addition and lower surface roughness. The surface roughness of Mg-Ti samples with 41, 51, and 58 at.% Ti increases and reaches a maximum value for the sample with 58 at.% Ti. As a result, the modulus and hardness of these samples are lower than the sample with 21 at.% Ti even though they are more Ti-rich. As Ti content increases to 81 at.%, the surface roughness of the $Mg_{0.19}Ti_{0.81}$ decreases. The effect of increased Ti content on the mechanical properties of this film is

apparent by the increased modulus and hardness values.

## Conclusion

Thin films of $Mg_{(1-x)}Ti_x$ alloys with different Ti content were deposited by magnetron co-sputtering techniques on Si substrates. XRD measurements showed that these alloys have a HCP structure. Moreover, the calculated lattice parameters of the $Mg_{(1-x)}Ti_x$ alloys follow Vegard's rule, indicating that single phase compounds were formed. AFM surface measurements showed that pure Mg thin film has the highest rms roughness while the alloy with ~ 20 at.% Ti has the smoothest surface. The in-plane particle size calculated from AFM height images was the largest (~ 750 nm) for the pure Mg film and fluctuates about a value of ~ 200 nm for the other films. Nanoindentation measurements showed that the alloy thin films have higher Young's modulus and hardness compared to pure Mg. In particular, the relatively smooth $Mg_{(1-x)}Ti_x$ alloy thin film with $x \sim 0.20$ displays the same improved mechanical properties as the alloy with $x \sim 0.80$ and thus has the potential of being used as a strong and hard protective coating.

## Acknowledgements

The authors thank M. Tessema for assistance with XRD measurements and R. Waldo for EPMA measurements.

## References

1. K. R. Baldwin, D. J. Bray, G. D. Howard, and R. W. Gardiner, "Corrosion behaviour of some vapour deposited magnesium alloys," *Materials Science and Technology*, 12 (1996), 929-944.

2. Y. Bohne, D. M. Seeger, C. Blawert, W. Dietzel, S. Mändl, and B. Rauschenbach, "Influence of ion energy on properties of Mg alloy thin films formed by ion beam sputter deposition," *Surface & Coatings Technology*, 200 (2006), 6527-6532.

3. T. Mitchell, S. Diplas, and P. Tsakiropoulos, "Characterisation of corrosion products formed on PVD in situ mechanically worked Mg-Ti alloys," *Journal of Alloys and Compounds,* 392 (2005), 127-141.

4. S. Rousselot, M. P. Bichat, D. Guay, and L. Roue, "Structure and electrochemical behaviour of metastable $Mg_{50}Ti_{50}$ alloy prepared by ball milling," *Journal of Power Sources,* 175 (2008), 621-624.

5. Y. T. Cheng, M. W. Verbrugge, M. P. Balogh, D. E. Rodak, and M. Lukitsch, "Magnesium-Titanium solid solution alloys," *United States Patent,* US 7651732B2, Jan. 26, 2010.

6. J. L. Murray, "The Mg-Ti (Magnesium-Titanium) System," *Bulletin of Alloy Phase Diagrams,* 7 (1986), 245-248.

7. W. P. Kalisvaart, H. J. Wondergem, F. Bakker, and P. H. L. Notten, "Mg-Ti based materials for electrochemical hydrogen storage," *Journal of Materials Research*, 22 (2007), 1640-1649.

8. R. A. H. Niessen and P. H. L. Notten, "Electrochemical Hydrogen Storage Characteristics of thin film MgX (X = Sc, Ti, V, Cr) Compounds," *Electrochemical and Solid-State Letters*, 8 (2005), A534-A538.

9. P. Vermeulen, H. J. Wondergem, P. C. J. Graat, D. M. Borsa, H. Schreuders, B. Dam, R. Griessen and P. H. L. Notten, "In situ electrochemical XRD study of (de)hydrogenation of $Mg_yTi_{100-y}$ thin films," *Journal of Materials Chemistry,* 18 (2008), 3680-3687.

10. B. Farangis, P. Nachimuthu, T. J. Richardson, J. L. Slack, B. K. Meyer, R. C. C. Perera, and M. D. Rubin, "Structural and electronic properties of magnesium-3D Transition metal switchable mirrors," *Solid State Ionics,* 165 (2003), 309-314.

11. D. M. Borsa, A. Baldi, M. Pasturel, H. Schreuders, B. Dam, R. Griessen, P. Vermeulen, and P. H. L. Notten, "Mg-Ti-H thin films for smart solar collectors," *Applied Physics Leters,* 88 (2006), 241910-1 – 241910-3.

12. T. J. Richardson, B. Farangis, J. L. Slack, P. Nachimuthu, R. Perera , N. Tamura, and M. Rubin, "X-ray absorption spectroscopy of transition metal magnesium hydride thin films," *Journal of Alloys and Compounds,* 356-357 (2003), 204-207.

13. P. Vermeulen, R. A. H. Niessen, and P. H. L. Notten, "Hydrogen storage in Metastable $Mg_yTi_{(1-y)}$ thin films," *Electrochemistry Communications,* 8 (2006), 27-32.

14. P. Vermeulen, R. A. H. Niessen, D. M. Borsa, B. Dam, R. Griessen, and P. H. L. Notten, "Effect of the deposition technique on the metallurgy and hydrogen storage characteristics of metastable $Mg_yTi_{(1-y)}$ thin films," *Electrochemical and Solid-State Letters,* 9 (2006), A520-A523.

15. G. Song, and D. Haddad, "The topography of magnetron sputter-deposited Mg-Ti alloy thin films," *Materials Chemistry and Physics,* accepted to be published.

16. W. C. Oliver and G. M. Pharr, "An improved technique for determining hardness and elastic modulus using load and displacement sensing indentation experiments," *Journal of Materials Research,* 7 (1992), 1564-1583.

17. R. A. Waldo, M. C. Militello, and S. W. Gaarenstroom, "Quantitative thin-film analysis with an energy-dispersive x-ray detector," *Surface and Interface Analysis,* 20 (1993), 111-114.

18. L. Vegard, "Die Konstitution der Mischkristalle und die raumfüllung der atome," *Zeitschrift für Physik,* 5 (1921), 17-26.

19. M. S. Bobji, S. K. Biswas, and J. B. Pethica, "Effect of roughness on the measurement of nanohardness –A computer simulation study," *Applied Physics Letters*, 71 (1997), 1059-1061.

20. J.Y. Kim, J.J. Lee, Y.H. Lee, J.I. Jang, and D. Kwon, "Surface roughness effect in instrumented indentation: A simple contact depth model and its verification," *Journal of Materials Research,* 21 (2006), 2975-2978.